Sentinel-1 InSAR Coherence for Land Cover Mapping: A Comparison of Multiple Feature-Based Classifiers

Alexander W. Jacob, *Member, IEEE*, Fernando Vicente-Guijalba, *Member, IEEE*, Carlos Lopez-Martinez, *Senior Member, IEEE*, Juan M. Lopez-Sanchez, *Senior Member, IEEE*, Marius Litzinger, Harald Kristen, Alejandro Mestre-Quereda, *Member, IEEE*, Dariusz Ziółkowski, Marco Lavalle, Claudia Notarnicola, *Member, IEEE*, Gopika Suresh, Oleg Antropov, *Member, IEEE*, Shaojia Ge, Jaan Praks, Yifang Ban, *Member, IEEE*, Eric Pottier, *Fellow, IEEE*, Jordi Joan Mallorquí Franquet, *Senior Member, IEEE*, Javier Duro, and Marcus E. Engdahl, *Member, IEEE*

***Abstract*—This article investigates and demonstrates the suitability of the Sentinel-1 interferometric coherence for land cover and vegetation mapping. In addition, this study analyzes the performance of this feature along with polarization and intensity products according to different classification strategies and algorithms. Seven different classification workflows were evaluated, covering pixel- and object-based analyses, unsupervised and supervised classification, different machine-learning classifiers, and the various effects of distinct input features in the SAR domain—interferometric coherence, backscattered intensities, and polarization. All classifications followed the Corine land cover nomenclature. Three different study areas in Europe were selected during 2015 and 2016 campaigns to maximize diversity of land cover. Overall accuracies (OA), ranging from 70% to 90%, were achieved depending on the study area and methodology, considering between 9 and 15 classes. The best results were achieved in the rather flat area of Doñana wetlands National Park in Spain (OA 90%), but even the challenging alpine terrain around the city of Merano in northern Italy (OA 77%) obtained promising results. The overall potential of Sentinel-1 interferometric coherence for land cover mapping was evaluated as very good. In all cases, coherence-based results provided higher accuracies than intensity-based strategies, considering 12 days of temporal sampling of the Sentinel-1 A stack. Both coherence and intensity prove to be complementary observables, increasing the overall accuracies in a combined strategy. The accuracy is expected to increase when Sentinel-1 A/B stacks, i.e., six-day sampling, are considered.**

***Index Terms*—Copernicus, interferometric coherence, land cover mapping, Sentinel-1, synthetic aperture radar (SAR).**

Manuscript received October 4, 2019; revised November 18, 2019; accepted November 23, 2019. Date of publication January 22, 2020; date of current version February 13, 2020. This work was supported in part by the European Space Agency via the ESA SEOM Program ITT under Grant AO/1-8306/15/I-NB "SEOM-S14SCI Land," in part by the European Commission under Grant 778360 for the possibility of funding exchange of researchers between DARES Technologies and EURAC Research with the H2020 Cost Action Project HERCULES, and in part by the Spanish Ministry of Science, Innovation and Universities, the State Agency of Research (AEI), and the European Funds for Regional Development (EFRD) under Project TEC2017-85244-C2-1-P. *(Corresponding author: Alexander W. Jacob.)*

A. W. Jacob, M. Litzinger, H. Kristen, and C. Notarnicola are with the Institute for Earth Observation, Eurac Research, 39100 Bolzano, Italy (e-mail: alexander.jacob@eurac.edu; marius.litzinger@gmail.com; haraldkristen@posteo.at; claudia.notarnicola@eurac.edu).

F. Vicente-Guijalba and J. Duro are with the Dares Technology, 08860 Barcelona, Spain (e-mail: fvicente@dares.tech; jduro@dares.tech).

C. Lopez-Martinez and J. J. Mallorquí Franquet are with the Signal Theory and Communication Department, Universitat Politécnica de Catalunya, 08034 Barcelona, Spain (e-mail: carlos.lopez@tsc.upc.edu; mallorqui@tsc.upc.es).

J. M. Lopez-Sanchez and A. Mestre-Quereda are with the Department of Physics, System Engineering, and Signal Theory, University of Alicante, 03690 Alicante, Spain (e-mail: juanma.lopez@ua.es; alejandro.mestre@ua.es).

D. Ziółkowski is with the Institute of Geodesy and Cartography, 02-679 Warsaw, Poland (e-mail: Dariusz.Ziolkowski@igik.edu.pl).

M. Lavalle is with the Jet Propulsion Laboratory, California Institute of Technology, Pasadena, CA 91109 USA (e-mail: marco.lavalle@jpl.nasa.gov).

G. Suresh is with the Federal Agency for Cartography and Geodesy, 60598 Frankfurt am Main, Germany (e-mail: gopika7787@gmail.com).

O. Antropov is with the VTT Technical Research Centre of Finland, 02044 Espoo, Finland (e-mail: oleg.antropov@vtt.fi).

S. Ge is with the School of Electronic and Optical Engineering, Nanjing University of Science and Technology, Nanjing, China (e-mail: geshaojia@njust.edu.cn).

J. Praks is with the Department of Electronics and Nanoengineering, School of Electrical Engineering, Aalto University, 02150 Helsinki, Finland (e-mail: jaan.praks@aalto.fi).

Y. Ban is with the Division of Geoinformatics, Department for Urban Planning and Environment, KTH Royal Institute of Technology, 11428 Stockholm, Sweden (e-mail: yifang@kth.se).

E. Pottier is with the Institut d'Electronique et de Télecommunications de Rennes, Universite de Rennes 1, 35000 Rennes, France (e-mail: eric.pottier@univ-rennes1.fr).

M. E. Engdahl is with the European Space Research Institute, European Space Agency, 00044 Frascati, Italy (e-mail: marcus.engdahl@esa.int).

Digital Object Identifier 10.1109/JSTARS.2019.2958847

I. Introduction

LAND cover classification and vegetation mapping are important applications of remote sensing data. In the frame of the GEO Task US-09-01a, the Group of Earth Observations (GEO) [1] addressed the identification of critical earth observation priorities considering land cover, vegetation and forest covers, and vegetation type or land use as observation priorities with an impact on different societal benefit areas (SBAs), such as, for instance, agriculture, ecosystems, or biodiversity. In addition, land cover classification and vegetation mapping are also important indicators of the interaction between humans and the natural environment. For instance, the use of this information in land use management plays a key role in the sustainable development and efficient exploitation of the earth's natural resources. Thus, the availability and accessibility of accurate and

timely land cover sets is critical at different spatial scales—at global or regional levels for policy-making and at a closer local scale to help farmers optimize their resources. For these reasons, land cover and vegetation mapping covers a broad perspective within the earth observation context.

The European Copernicus Programme, and in particular, the Copernicus Land Monitoring Service (CLMS) provides the framework for such an approach. The space segment of the programme, the Sentinels, defines a whole new playground for exploring the limits and potentialities of diverse technologies in order to generate updated and precise land cover maps all around the globe. In this context, synthetic aperture radar (SAR) technology is able to provide data during the day and night and in cloudy conditions. Consequently, these systems may deliver systematic and reliable temporal data records of an observed area of the earth's surface. Since its launch in April 2014, the C-band Sentinel-1A system has been providing SAR data time series with a 12-day repeat cycle. The launch of a twin C-band satellite Sentinel-1B system in April 2016 has reduced this to a six-day repeat cycle. In addition, thanks to the interferometric capabilities, the temporal information is captured not only in the time series of SAR images, but also in the interferometric coherence from pairs of SAR images. The availability of these global data favours the emergence of alternative approaches to the mapping scene where mostly the optical, but also the radiometric, data have established their niche. In this regard, the purpose of this article is specifically to explore and evaluate performance when using the interferometric coherence from SAR, and in particular Sentinel-1, time series and interferometric data for land cover and vegetation mapping. Using SAR data for land cover mapping is not a new concept and attempts to use it go back to the time of the ERS-1 mission, e.g., [2], [3], but only a small number of classes were detectable then, due to the constraints of the available imagery at the time.

The first objective is to quantify the impact of using Sentinel-1 InSAR (interferometric SAR) data relative to traditional SAR-based land cover and vegetation mapping [4]–[7]. Previous literature have already indicated the usefulness of using InSAR information for land cover classification [8]–[16]. In addition to the impact of interferometric coherence, this article also evaluates the impact, in terms of land cover classification and vegetation mapping, of SAR intensity and SAR polarimetry [17]–[19].

Classification performances also depend on the methodology employed to process the data. Thus, the second objective of this article is to evaluate the impact of the classification technique, as well as different aspects associated with it. Consequently, seven different classification techniques are evaluated, where aspects such as the use of pixel or segment-based approaches or the impact of the sampling strategy on training are also considered.

The evaluation of the classification performances is achieved considering three different Sentinel-1 SAR data time series in 2015 and 2016 campaigns at test sites in Spain, Italy, and Poland. These three areas range from barren land, crops, or urban areas to high-altitude alpine environments. The complete evaluation was conducted as part of the European Space Agency project SEOM-S14SCI Land "SinCohMap: Exploitation of Sentinel-1 InSAR Coherence for Land-Cover and Vegetation Mapping" (www.sincohmap.org).

This article is structured as follows. Section II provides a formal description of the interferometric coherence and its relation to the land cover along with the matrix formulation to consider multitemporal stacks. The data setup and the classification strategies exploited are also introduced in this section. Section III introduces the obtained classification results with the different methodologies. In Section IV, a discussion and insights from the obtained results are presented. Finally, in Section V, conclusions and future perspectives are provided.

II. Materials and Methods

A. Multitemporal Coherence Matrix

The complex correlation coefficient between two complex SAR images S_1 and S_2 represents the normalized correlation between these two SAR acquisitions and is mathematically obtained by

$$\rho = |\rho| e^{i\phi} = \frac{E\{S_1 S_2^*\}}{\sqrt{E\left\{|S_1|^2\right\} E\left\{|S_2|^2\right\}}} \tag{1}$$

where $E\{\cdot\}$ represents the mathematical expectation and * indicates the complex conjugate. Typically, the complex phase is interpreted by means of the amplitude $|\rho|$, or coherence, and the phase ϕ corresponding to the interferometric phase. While the phase term is mostly related to the geometrical aspects of the scene and the acquisition system, the coherence is customarily described as the combination of multiplicative set of decorrelating factors as follows [20]–[22]:

$$|\rho| = \rho_{\text{temporal}} \rho_{\text{SNR}} \rho_{\text{range}} \rho_{\text{volume}} \rho_{\text{other}}. \tag{2}$$

Although some terms depend on the system or external parameters, i.e., ρ_{SNR}, ρ_{range}, and ρ_{other}, others depend on the scatterer under observation [20]–[22]. In this work, attention is focused on the latter ones, which will justify a classification approach based on coherence as the input feature. Regarding the temporal decorrelation term ρ_{temporal}, this is the most important decorrelation term in the frame of this study, as it is expected to be able to provide information about the evolution of the land cover in the scene over temporal series of S-1 data with possibly increasing temporal baselines, i.e., the time span between both acquisitions. With respect to the volume decorrelation term ρ_{volume}, in the case of Sentinel-1, the nominal orbital tube is 50 m (RMS), thus the small normal baselines in the repeat-pass configuration of this system prevents the volumetric decorrelation from being a term of significant interest.

Under the assumption of ergodicity and considering locally stationary processes, the spatial averaging around the pixel of the study leads to the maximum likelihood estimator of the coherence [23], which can be expressed for each spatial pixel as

$$\hat{\rho} = \frac{\sum_{i=1}^{L} S_1(i) \cdot S_2^*(i)}{\sqrt{\sum_{i=1}^{L} |S_1(i)|^2 \sum_{i=1}^{L} |S_2(i)|^2}} \tag{3}$$

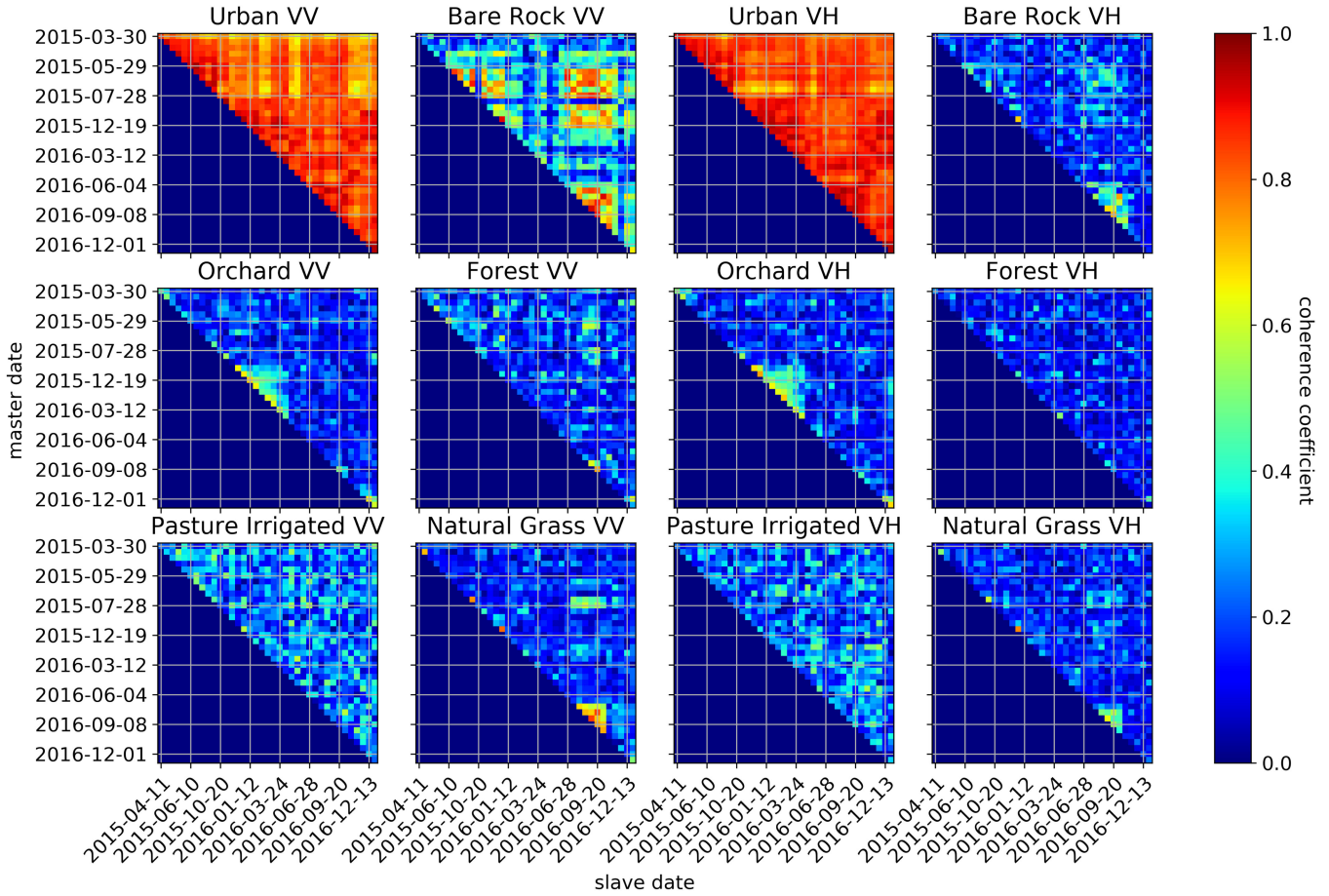

Fig. 1. Comparison of the dynamics of multitemporal coherence matrices in six different land cover types (urban, bare rock, orchards, forest, pasture irrigated, natural grassland) in the Merano study area, containing all possible combinations of temporal baselines for the six selected pixels of the six different land cover types. Left: VV polarization, right: VH polarization.

where L indicates the spatial set of samples employed to compute the estimated correlation. When a time series of N SAR images is available, the potential combinations of pairs of SAR images to derive the corresponding complex correlation coefficients is equal to $N \cdot (N-1)/2$, and it is possible to define the Hermitian positive semidefinite temporal covariance matrix for the complete interferometric stack as follows:

$$\hat{C}_{\text{temporal}} = \begin{bmatrix} \langle |S_1|^2 \rangle & \langle S_1 S_2^* \rangle & \cdots & \langle S_1 S_N^* \rangle \\ \langle S_2 S_1^* \rangle & \langle |S_2|^2 \rangle & \cdots & \langle S_2 S_N^* \rangle \\ \vdots & \vdots & \ddots & \vdots \\ \langle S_N S_1^* \rangle & \langle S_N S_2^* \rangle & \cdots & \langle |S_N|^2 \rangle \end{bmatrix}. \quad (4)$$

The multitemporal covariance matrix in (4) contains, on the main diagonal, the sequence of backscatterer intensities, and the off-diagonal terms contain all possible temporal interferometric combinations of the SAR stack of images. Assuming a constant image acquisition sampling, the closer the interferometric combination is to the mean diagonal, the shorter the temporal baseline. Each of the diagonals represents an isobaseline stack. Applying a proper power normalization, the multitemporal coherence matrix can be obtained from (4) as

$$\Gamma_{\text{temporal}} = \begin{bmatrix} 1 & \rho_{12} & \cdots & \rho_{1N} \\ \rho_{12}^* & 1 & \cdots & \rho_{2N} \\ \vdots & \vdots & \ddots & \vdots \\ \rho_{1N}^* & \rho_{2N}^* & \cdots & 1 \end{bmatrix}. \quad (5)$$

The information contained in (5) is a subset of the information contained in the more general covariance matrix but it allows the interferometric coherence to be isolated from the rest of the information. The most relevant advantage of using both the covariance or coherence matrix formulation is that it not only allows a more detailed characterization of the target under observation, but also a better characterization of its dynamics. The information provided by these matrices is the starting point for the classification strategies described in the following sections.

As an example, in Fig. 1, the upper half (with the lower part symmetrical) of the multitemporal coherence matrix expressed in (5) is provided for six different land cover types—urban, bare rock, orchard, forest, and irrigated grassland in medium and in high altitudes. This set of figures illustrates the variability along the internal time dimensions, i.e., off-diagonals for equibaseline

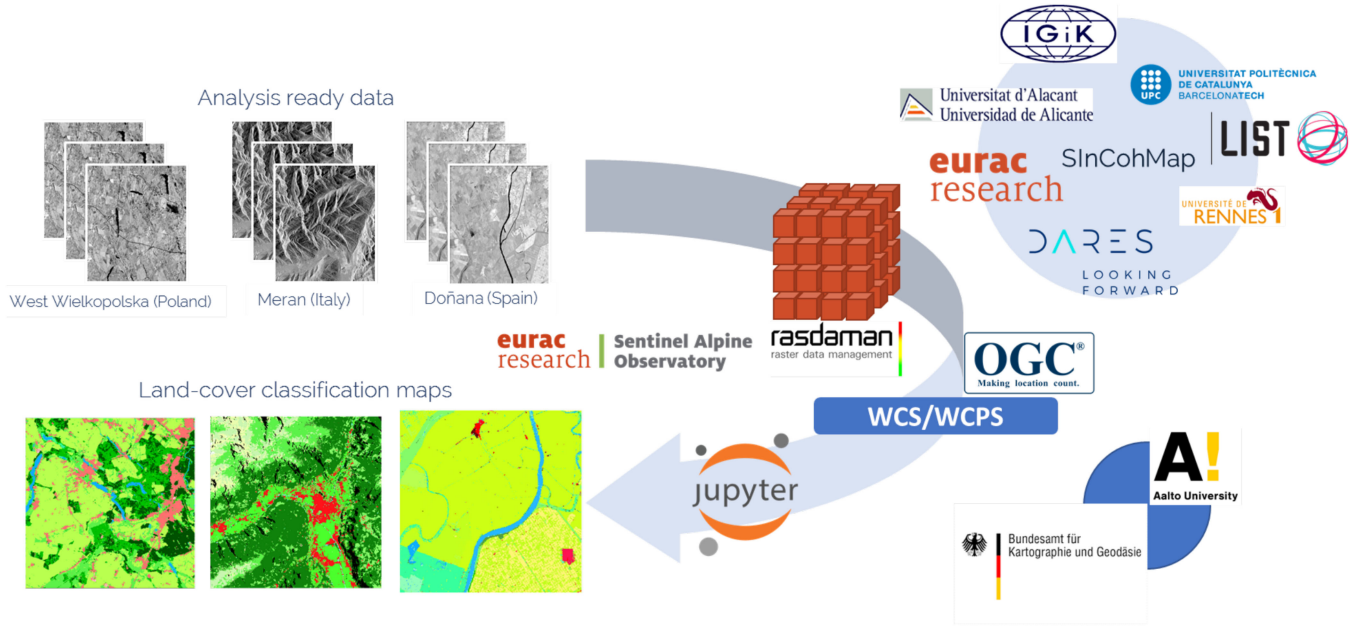

Fig. 2. Diagram of the RR experience from the analysis-ready data to land cover classification maps. All data are stored and can be accessed by all participants, internal and external teams, exploiting the data allocated in datacubes via OGC standard protocols such as WCS/WCPS. Methodological approaches are developed in python Jupyter notebooks [24], [25], which allow the participants to focus strictly on the development of their classification methods.

coherences and rowwise for equireference coherences, for each present class. The way in which the coherence evolves in a different way for each class is clearly visible, with the most stable that is observed for the urban context. In the other cases, the land dynamics, such as the decorrelation periods due to snow in the bare rock areas or the cultivation cycles in the orchards or agricultural sites, drive the behavior of the coherence matrices in a more complex manner. The polarimetric diversity of the aforementioned land covers, illustrated here with both polarimetric channels VV (on the left) and VH (on the right), also supports the use of the polarimetric information in the classification scheme. For instance, coherence over bare rock is significantly lower at the VH channel than at the VV channel as a consequence of the low backscattered power at VH from the rock surface, which yields an important decorrelation due to a low signal-to-noise ratio, i.e., ρ_{SNR} in (2) is smaller at VH than at VV for bare rock.

B. Round-Robin Consultation Experience

The evaluation was initiated by a round-robin (RR) exercise within the context of the ESA SEOM SInCohMap project (see Fig. 2). The RR included in its definition the evaluation of multiple classification methodologies for land cover and the intercomparison of the results obtained from the perspective of each methodology. The idea was not only to involve the different teams and partners of the project in the comparison, but also to provide external scientists and experts in the field the possibility to participate. The final objective was to shed some light onto the characteristics and features that a classification method based on interferometric coherence products should consider. Fig. 2 provides an overview of the main elements involved and the required setup defined in the exercise. In this section, details on each of these elements are provided.

The first step to providing a significant methodological comparison is to ensure that all methods are using the same stack of input data, otherwise the outcome of the comparison would not be reliable. Therefore, analysis-ready data were provided to all participants. Moreover, the InSAR data processing, especially involving the Sentinel-1 single look complex (SLC) interferometric wide swath (IW) mode is not straightforward. References to the steps involving the interferometric processing chain can be easily found in the literature [26]. Nonetheless, precise coregistration strategies shall be addressed in order to satisfy the requirements of the S-1 IW products [27]. To satisfy the quality and homogeneity of the comparison, the SLC data were processed to produce a single InSAR stack using the in-house software PRISAR [28], developed and maintained by UPC and DARES. The steps and parameters during this stage are:

1) coregistration, using precise orbital information and an external DEM;
2) radiometric calibration, to compensate topographical distortions and bias, enabling the use of the radiometric backscatter and intensity features;
3) interferometric stack generation, providing all the possible combinations between the SLC acquisitions of 2015 and 2016;
4) speckle filtering and coherence estimation; exploiting a box-car filter with four samples in azimuth and 19 samples in range;
5) geocoding, creating a WGS84 UTM grid for all of the interferometric products.

The resolution of the final product is 60 m $\times$ 80 m. To prevent issues in the geocoding transformation, this is oversampled by a

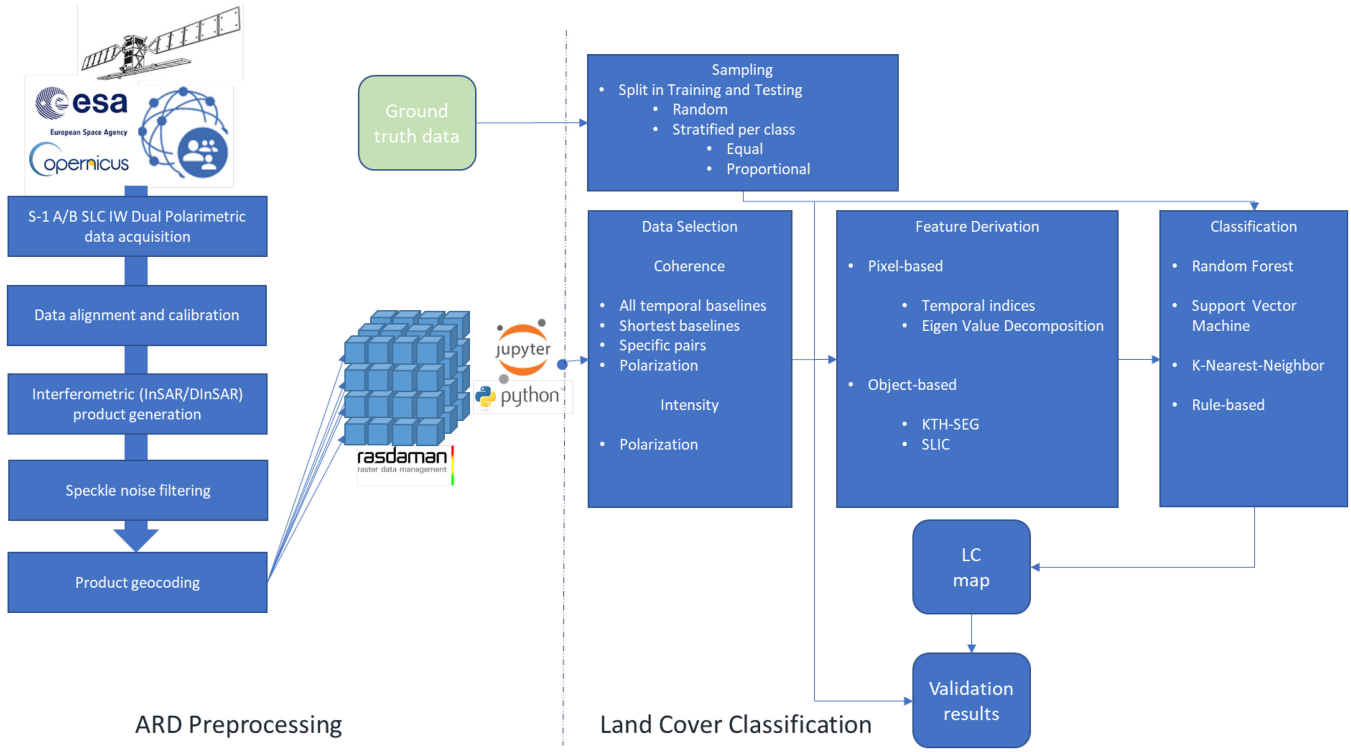

Fig. 3. Overview of the processing workflow. The left-hand side shows the preprocessing steps for creating the analysis-ready SAR products and the right-hand side the steps used in the various approaches, implemented by the participants of the rr exercise.

factor of 3 × 4. Thus, for all sites, a UTM grid of 1000 × 1000 samples of 20 × 20 m resolution was defined, resulting in an area of 20 × 20 km for each site.

Despite processing small areas, the dataset produced by InSAR processing is huge. All possible interferometric combinations consist of more than 700 combinations in the considered sites. Moreover, the consideration of the two channels from the polarimetric domain significatively increases the size of the stack. To simplify and provide access to this amount of information, all the InSAR data for a particular site were grouped together to form a 5-D datacube—two dimensions for space (easting and northing), two dimensions for time (master and slave dates of the interferogram), and one additional dimension for the polarimetric channel. The datacubes with the InSAR data, along with the corresponding ground truth reference information were uploaded to a server with geographical capabilities (rasdaman). Standard protocols for accessing and querying the data were also offered, such as WCS and its extension, the WCPS.

The processing requirements to deal with all the data stack are also demanding in terms of hardware infrastructure. To engage and simplify participation in the RR, a processing environment was set up for each of the participants of the experience [29] on the infrastructure of the Eurac Research Sentinel Alpine Observatory (http://sao.eurac.edu) operated by the Institute for Earth Observation. The aforementioned datacubes were organized in rasdaman [30], [31] and made openly accessible. On top of this, a Jupyter-hub environment was set up for all participants to have a web-accessible (http://sincohmap-hub.eurac.edu) processing environment executing all code right next to the data. In this context, the use of Jupyter notebooks [24], [25] has proven to be a really simple way to develop prototypes and methods. The fast access to the already processed data served to develop and test a wide variety of methods rapidly. With this setup, the context for an efficient and reliable comparison was defined. A total of six teams were engaged into the RR, including two external participants, and during the five months of evaluation, seven different classification methodologies were considered in the results comparison.

C. *Land Cover Classification Methodologies*

In this section, the seven methodologies proposed and tested by the participants during the RR are described. Fig. 3 shows the implemented workflows, described in detail in this section.

1) Random Forest Classification (RF): The first methodology consists of a supervised classification approach [32] based on the random forest (RF) algorithm [33]. In this approach, the selected features are the Sentinel-1 image intensities and the interferometric coherences with the shortest temporal baselines. Thus, the coherence between consecutive images was analyzed assuming they are less affected by temporal decorrelation and providing more information about changes occurring in the different land covers with different intensities and/or different times of the year. This information corresponds to the main diagonal of values in the depicted coherence matrix for selected pixels in Fig. 1. Limited tests have also been performed exploiting longer temporal baselines.

2) Eigenvalue Classification (EigCoh): In this methodology, a linear transformation of the original space is performed before the classification step itself is applied. In this case, the input feature is the whole coherence matrix, i.e., all the interferometric coherence combinations, and before being classified, the data are decomposed using the eigenvalue decomposition theorem. To exploit the backscattering information, the intensity products are, either together with the coherences or by themselves, also transformed by the eigendecomposition algorithm before entering the classifier. This method exploits the transformed space to train and classify exploiting the the multitemporal coherence and/or intensity eigenvalues using an RF classifier. This method permits the dimensional space to be reduced from the data information perspective. One percent of the overall image size was randomly sampled as training samples proportional to the class size of the ground truth data.

3) Temporal Dynamic Indices (TDI): Building up on intra-annual indices used for land cover classification [34], [35] this method exploits the temporal dynamics of coherence data. Assuming that every land cover class has its own spectral behavior over time, values from the available coherence time series were used to generate several indices, reflecting these temporal dynamics. From each coherence matrix of every single pixel, the values of the baseline evolution of the first master date (first row of matrix) and the evolution of the shortest baseline (first diagonal) were extracted as time series. For these two series of values, minimum, maximum, and mean values and the slope between the first and last value were calculated as separate indices. Further, a univariate spline and an interpolated univariate spline [36] with a smoothing degree of $k = 1$ were fitted to calculate the first derivative and an integral. The best fitting polynomial [37] function for the time series was calculated to use its fitting degree and the mean and steepest slope. Finally, a Lomb–Scargle model [38], [39] was generated to use the maximum and minimum power of the periodogramm and the time step of the maximum power. Also, seasonal three-month averages and normal coherence images were generated for the coherence time series. The derived indices were used as features for the supervised training of an RF model. One percent of the overall image size was randomly sampled as training samples proportional to the class size of the ground truth data [40], [41].

4) Object-Based Image Classification (KTH-SEG): An image segmentation using an edge-enhanced region growing and merging approach was used in conjunction with an object feature-based support vector machine classifier [7]. This methodology was applied to a number of different input feature stacks derived from the multitemporal interferometric coherence amplitude matrix and/or intensities derived from Sentinel-1 A. All results presented are based on the shortest temporal baseline diagonal of the matrix. Different sample sizes were tested (0.01% or 100 pixels, 0.1% or 1000 pixels, and 1% or 10000 pixels) where the number of training samples was held constant for each class. When matching pixel samples to a segment, the decision is based on the majority of pixels belonging to one class, in the event that more than one pixel falls into a segment. However, this case occurred rarely, as the sampling was stratified based on the polygons of the reference data, and rules were imposed such that pixels selected for sampling were not too close to each other. A number of different segment sizes were tested and the best results were found when limiting segments to fall in the range of 8 to 500 pixels, where homogeneity criteria were equally weighted and where the canny edge detector, as described in [42, ch. 4.2.1], was applied. Comparisons were also made running the same input feature stacks on a pixel-based classification approach based on RFs, as described above.

5) Superpixel Segmentation and k-Nearest Neighbors (kNN)-Based Labeling Classification (SPKnnLab): This classification approach is represented by an unsupervised segmentation procedure followed by distance-based labeling. In the first stage, an unsupervised image segmentation is performed using image features calculated from original interferometric SAR coherence stacks. The VV and VH interferometric coherence scenes were combined together as a single stack to provide an input to the principal component analysis (PCA) procedure. Image features were normalized using the histogram equalization approach [43]. Three primary principal components were used as image features in a superpixel segmentation implemented using a simple linear iterative clustering (SLIC) approach [44]. In the second stage, delineated homogeneous areas were labeled. We used a limited yet representative sample of reference/training data systematically sampled over the training areas. While few superpixels could be labeled directly using this sample of reference data, to label other superpixels, we adopted the kNN classification approach, described in, e.g., [45]. Euclidean distance in the normalized space of image features was used to calculate distances between neighbors in the kNN approach. The most suitable value of $k = 25$ was decided by analyzing the classification performance on the training dataset.

6) Expert Knowledge Decision Tree Classification (EKDT): The methodology is based on the set of various average coherence images generated from the original coherence matrix. The main idea behind using averaged images by selecting the highest coherence data was to remove as much as possible the effects of the decrease in coherence associated with weather conditions (rain, snow) and changes in soil and vegetation moisture. However, the use of averaged data reduces the noise present in the coherence images. As a good compromise, averaging ten images under relatively dry conditions and not affected by moisture changes provides a significant noise reduction. Considering smaller subsets for averaging, e.g., four images, enables us to better track the agricultural areas. First, the averages were generated from all coherence images of each coherence interval (12, 24, 36 days, etc.) separately for VV and VH polarizations. In the next step, for 12- and 24-day coherence intervals, four and ten images with the highest coherence from summer and winter seasons are selected and averages are generated. Winter and summer averaged images selected as agricultural area were covered either by bare soil (high coherence) or vegetation (low coherence) during these two seasons, respectively. During the spring and autumn, we can expect to have a mixture of both. The methodology is prepared based on the expert knowledge of the behavior of the coherence during each season on the

TABLE I
SUMMARY OF METHODOLOGIES DURING THE RR CONSULTATION AND MAIN FEATURES

Methodology	Space object	Decision type	Baselines	Pol. channels	Intensity
RF	Pixel	RF ML classifier	short	VV & VH	YES
EigCoh	Pixel	RF ML classifier	full mat.	VV & VH	YES
TDI	Pixel	RF ML classifier	short & long	VV & VH	YES
KTH-SEG	Object	SVM classifier	short & long	VV & VH	YES
SPSegKnnLab	Object	kNN ML classifier	full mat.	VV & VH	NO
EKDT	Object	Decision Tree	short	VV & VH	NO
DARB	Object	Decision Threshold	reduced set	VV & VH	NO

Short-shortest temporal baselines, long-long temporal baselines full mat.-full multitemporal coherence matrix.

West Wielkopolska (Poland) site. The same set of coherence averages are selected for the classification on the other test sites—Doñana (Spain) and Merano, South Tyrol (Italy). The decision tree method [46] is selected for classification as it is expected that various input images will be the best for the classification of particular land cover classes. The different trees have been built for particular test sites to obtain the best possible results.

7) Data Adaptive Rule-Based Classification (DARB): DARB is a data-adaptive technique as the thresholds for classification depend on the histograms of the image and, hence, on a data-dependent approach. From the total amount of interferometric products, ten coherence pairs from each site were chosen for this analysis, five with shorter temporal baselines, and five with longer baselines. The coherence ranges in images with shorter baselines was overall higher than those with longer baselines. The coherence values exhibited by the land cover classes of forest, agriculture, water, and wetlands were also observed to be more distinguishable in coherence images made by images with shorter temporal baselines. The VV and VH coherence pairs were downloaded and analyzed separately. The histogram of the image is first analyzed to check whether the image histogram is monomodal or bimodal and Gaussian curves were fit accordingly. The original coherence values were not changed and, hence, no extra uncertainties were induced by this process. In cases where the histogram was homogeneous and could be fitted with a single Gaussian curve, the peak of the histogram (mean; t_0) represented the coherence value of the most dominant land cover class. In our dataset of 30 images (ten for each site), images with heterogeneous distributions or with bimodal histograms were fit with two Gaussian curves. The coherence values corresponding to the peaks of the two simulated curves (t_1 and t_2) along with the mean coherence values (t_0) were used as thresholds to divide the image into four classes. For images with monomodal histograms, the value of t_0 (mean) is known. However, to extract t_1 and t_2, two Gaussian curves were simulated for these data as well. Once the thresholds for image classification were extracted, the image was segmented into different clusters using the agglomerative clustering technique [33] with the number of clusters set to 80. Once segmentation was complete, the mean coherence in each segment was considered and the segments were assigned classes based on the previously extracted thresholds (t_0, t_1, and t_2; see equations below). The thresholds used for classification in the DARB method are given as follows, with the classes representing the corresponding CORINE land cover (CLC) level 3 class numbers:

$$\gamma \leq t_2 = 100$$
$$t_0 \geq \gamma > t_2 = 200$$
$$t_1 \geq \gamma > t_0 = 300$$
$$t_1 \geq \gamma = 400.$$

Most of the strategies are able to incorporate information from the different polarimetric channels simultaneously or independently during the classification. Moreover, the temporal series of image intensities can also be included in the classification stage. These possibilities are essential to test and analyze the impact of the different features. As a summary, Table I provides a comparable overview of the main features involving all the evaluated methodologies.

D. Test Sites and Datasets

Three different locations have been selected for the RR experience. The site selection process considered overlapping the different cover types but in alternative geographical locations and under different circumstances, so the overall conclusions of the analysis are expected to be much less site dependent. A brief description of each site is provided in this section.

- *Site 1: Doñana (Spain).* A specific test site for agriculture, wetlands, and related land covers close to Seville in the SW of Spain. The pilot area is centred at 37°08'N, 06°07'E. At the southeast of the rice fields, there is a wide area of different crops, including wheat, cotton, barley, corn, peas, sugar beet, lentils, potatoes, etc.
- *Site 2: Merano, South Tyrol (Italy).* South Tyrol is an autonomous province in northern Italy located in the center of the Alps with steep elevation gradients stretching from 190–3890 m a.s.l. The area is very dynamic in terms of temporal and spatial variability of land cover. Overall, 44% or 3228 km^2 of the South Tyrol region is covered by forest. The pilot area is centred at 46°40'N, 11°09'E. The area around Merano was chosen due to its large variability of land cover, ranging from urban areas in the valley floor to glacier areas above 3000 m a.s.l.
- *Site 3: West Wielkopolska (Poland).* The study area in Poland is located in the west part of Poland within a region

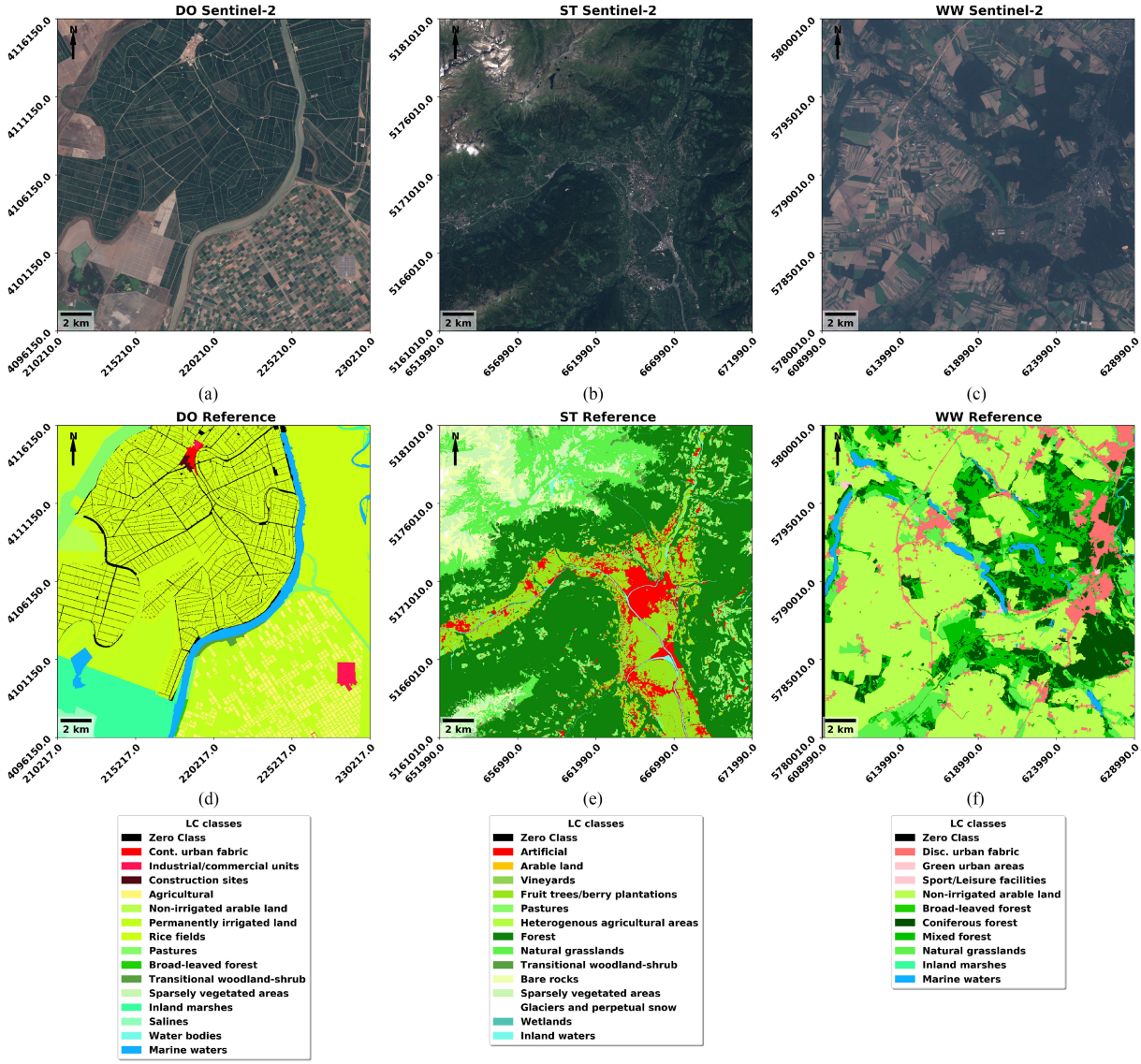

Fig. 4. RGB optical images over the regions of interest in: (a) Doñana (Spain), 2016-07-16; (b) Merano, South Tyrol (Italy), 2016-08-07; and (c) West Wielkopolska (Poland), 2016-09-13. Illustration of the ground truth reference data in the CLC level 3 for the correspondent site in (d) UTM Zone 30 N, (e) UTM Zone 32 N, and (f) UTM Zone 33 N.

with well developed agriculture, dominated by intensively used large fields with areas above 10 ha. The dominating crops are wheat, rye, triticale, barley, oats, rape, corn, and sugar beet. This site is also occupied by alfalfa and grasslands. The pilot area, centred at 52°14'N, 16°48'E, contains three sites representing different land cover types mainly composed of agriculture, forest, and urban areas.

For each location, an area of interest (AOI) of 20×20 km is selected where land cover ground truth information is available in the CLC level 3 nomenclature. The total number of classes varies per site, and it goes from 15 for Doñana, 15 for Merano, South Tyrol, and nine for the West Wielkopolska site. The zero class was also considered in this number, providing a representation for the samples outside of the original definition of the ground truth data in the case of the Doñana area and a representation of areas affected by strong a layover and foreshortening due to the topography present in the case of the South Tyrol study area. This class also helps the classification methods to provide samples beyond the original definition. As a visual reference, an optical overview of the locations and the overlaid ground truth is illustrated in Fig. 4.

Following the steps described in Section II-B, the AOI of each site is processed to generate the multitemporal coherence data considering the stable available S-1 SLC IW acquisition mode. The period of time and the amount of preprocessed data considered per site are summarized in Table II. It must be remarked that the operational ramp-up acquisition phase for the Sentinel-1 provided a different starting acquisition date for each considered date. In the case of the South Tyrol site, it was detected that additional modes, as stripmap, and polarizations (transmission of the horizontal polarized signal) were acquired, instead of the inland by default IW swath, vertical polarization transmission. This is the reason why the stack in this case shows fewer images than the other two.

TABLE II
SUMMARY OF THE DATASET STRUCTURE: RELATIVE ORBIT NUMBER (RON), ORBITAL PASS IN ASCENDING (ASC) OR DESCENDING (DSC) MODES, PERIOD OF OBSERVATION BETWEEN INITIAL AND FINAL DATES AND THE NUMBER OF ACQUISITIONS (SLC) INVOLVED AND INTERFEROGRAMS GENERATED AT EACH SITE

Site location	RON	Orbit pass	Initial date	Final date	No. SLC	No. interferograms
Doñana	154	DSC	20150309	20161228	49	1176
Merano, South Tyrol	117	ASC	20150330	20161225	38	703
West Wielkopolska	175	ASC	20150109	20161229	55	1485

III. RESULTS

During the RR exercise, all the methodologies presented in Section II were evaluated utilizing the three datasets described. Some of the methodologies were tested using the interferometric coherence and intensities alone, while, in other cases, intensities and coherence were used simultaneously. A systematic accuracy assessment is performed across all the classification maps produced in this article. The overall accuracy is the selected parameter employed to summarize and compare the performances of each methodology and parametric combination. Although any parameter summarizing a classification from the confusion matrix must suffer from different sorts of inconsistencies [47], in this case, the comparisons are performed within the same sites, i.e., the class distribution remains equal from one methodology to another. This fact enables us to securely exploit the overall accuracy (OA) as a simple and relative parameter used to compare realizations. In Table III, a summary with all the obtained OA is provided. The summarized results in Table III are further discussed in Section IV. Such an analysis involved the generation of the confusion matrix [47] per site and per strategy. Figs. 5 and 6 provide a sample of the confusion matrices obtained for the results at the Doñana and Merano sites. In Fig. 5, one can see that most classes are identified accurately, with detection rates over 80%. In some cases, such as agricultural and permanently irrigated land, however, one can see confusion between those classes reaching up to 30%. In the case of Merano in Fig. 6, the level of confusion is considerably higher. One can see, e.g., a cluster of confusion between the bare rocks, sparsely vegetated areas and glaciers and perpetual snow classes, all mostly present in high altitudes and hence, affected by considerable periods of snow cover during the annual cycle of the seasons. In Fig. 7, results from the eigenvalue classification at the Donana site are shown. Fig. 8 shows a comparison between pixel-based and object-oriented classification for each test site.

IV. DISCUSSION

In the previous two sections, a number of very different classification methodologies were described and their classification accuracies presented. While each of those methodologies merits their own discussion, the following discussion focuses on the common aspects that can be derived regarding the main objectives of this research, the suitability of interferometric coherence amplitudes for land cover mapping. Those common aspects of the classification processing chain are discussed separately including the impact of using VV or VH polarization, or both, working only with backscatter intensity or coherence or both, applying pixel or object-based classification, the number of samples used for training a machine-learning algorithm, and how much information is needed from the coherence matrix in order to provide reasonable results. As stated in Section II-B, the spatial resolution space of the results is limited by the interferometric coherence product. The original sensor resolution is degraded by the coherence estimation strategy, a box-car window in this case, providing a larger resolution of approximately 80 m. Thus, the minimum detectable object is defined by the product resolution itself, which may result in classification bias, specially in small or boundary areas. For instance, this is clearly visible in the crop field area in the southeast part of the Doñana site. Nonlocal and advanced adaptive coherence estimation strategies [48]–[51] could help to preserve object definition, especially in case of point targets and image details in which coherence is high (i.e., wherever the coherence estimation is not biased due to a low number of samples). This specific aspect constitutes a future study and is left out of the present article in which the main aim is to show how the use of coherence improves terrain classification. Nonhomogeneous coherence estimation strategies could help to preserve object definition but might incur in coherence estimation bias due to the low number of samples. Outside the scope of this analysis, a future evaluation focused on this matter will help to provide a solid conclusion.

A. *Effects on the Length of the Temporal Baseline*

The impact of the temporal baselines considered from the coherence matrix for classification has been studied in rows 7–14 of Table III. What can be seen is that the impact of including more baselines is very limited in most cases. Only in one study area, the one in Merano, South Tyrol, did the inclusion of more than the shortest baseline lead to significant improvements of the results. Both in Doñana and West Wielkopolska, there was no effect visible when including more data from the temporal domain. Also in Merano, there was no significant improvement after the two second-shortest baselines, including 12- and 24-day temporal baselines. When looking into the multitemporal signatures of various land cover types as presented in Fig. 1, one can also clearly see that for most land cover types, the signal gets noisier and weaker the further away from the shortest baseline diagonal one gets.

B. *Intensity Versus Coherence-Based Classification*

When deciding which features to use for land cover classification based on SAR imagery, backscatter intensity is, of

TABLE III
RESULTS SUMMARY FOR THE EVALUATION PERFORMED WITH THE DIFFERENT METHODOLOGIES AND FEATURES SETUP

id	Method.	Input data	Training samples	Space obj.	max. B_{temp}	Pol.	OA DÑ (%)	OA ST (%)	OA WW (%)
1	RF	Int. + Coh.	1 %	Pixel	12	VV	79.4	-	-
2		Int. + Coh.	1 %	Pixel	12	VH	77.4	-	-
3		Int. + Coh.	1 %	Pixel	12	VV+VH	80.2	-	-
4		Int.	1 %	Pixel	-	VV	61.2	-	-
5		Int.	1 %	Pixel	-	VH	61.0	-	-
6		Int.	1 %	Pixel	-	VV+VH	62.4	-	-
7		Coh.	1 %	Pixel	12	VV+VH	74.2	65.2	70.0
8		Coh.	1 %	Pixel	24	VV+VH	74.4	68.9	70.0
9		Coh.	1 %	Pixel	36	VV+VH	74.3	68.9	70.2
10		Coh.	1 %	Pixel	48	VV+VH	73.6	69.0	70.1
11		Coh.	1 %	Pixel	60	VV+VH	73.6	69.3	70.1
12		Coh.	1 %	Pixel	72	VV+VH	73.3	69.5	70.0
13		Coh.	1 %	Pixel	84	VV+VH	72.5	69.1	70.1
14		Coh.	1 %	Pixel	96	VV+VH	72.9	69.4	69.9
15	EigCoh	Coh.	1 %	Pixel	Full mat.	VV	78.2	70.9	71.0
16		Coh.	1 %	Pixel	Full mat.	VH	74.5	68.8	67.4
17		Coh.	1 %	Pixel	Full mat.	VV+VH	79.8	72.5	71.7
18		Int.	1 %	Pixel	-	VV	74.6	54.9	64.0
19		Int.	1 %	Pixel	-	VH	74.0	56.1	66.9
20		Int.	1 %	Pixel	-	VV+VH	77.8	58.9	69.5
21		Int. + Coh.	1 %	Pixel	Full mat.	VV	81.9	72.0	73.2
22		Int. + Coh.	1 %	Pixel	Full mat.	VH	79.8	70.9	71.7
23		Int. + Coh.	1 %	Pixel	Full mat.	VV+VH	83.3	73.8	75.0
24	TDI	Coh.	1 %	Pixel	12	VV	82.1	72.3	73.3
25	KTH-SEG	Int. + Coh.	1 %	Pixel	12	VV+VH	76.8	71.7	72.6
26		Int. + Coh.	1 %	Object	12	VV+VH	84.1	77.0	77.0
27		Coh.	0.01 %	Object	12	VV+VH	74.3	56.8	54.1
28		Coh.	0.1 %	Object	12	VV+VH	79.7	65.9	71.8
29		Coh.	1 %	Object	12	VV+VH	85.7	69.3	77.0
30	SPKnnLab	Coh.	1 %	Object	12	VV+VH	90.3	76.5	79.6
31	EKDT	Coh.	1 %	Pixel	12	VV+VH	$78.7^{\dagger}$	$83.5^{\dagger}$	$87.0^{\dagger}$
32	DARB	Coh.	1 %	Object	12	VV+VH	51.4	68.2	59.4

The features analyzed involve the classification strategy or methodology, the input data type, the number of samples used for training, the spatial objects employed, the maximum temporal baseline (B_{temp}) considered, and the polarimetric channels involved. The overall accuracies (OA), in percentage, provide a recap of the performance of each evaluation at each test site—Doñana (DÑ) with 15 classes, South Tyrol (ST) with 15 classes, and West Wielkopolska (WW) with nine classes. Evaluation on ST and WW with RF and Int./Int+Coh were not performed (–) as specific evaluations outside the scope of this study were performed instead. (Note † OA produced for CLC Level 1, i.e., five classes)

course, the most obvious choice due to its higher availability, and the fact that it is already preprocessed and downloadable in the Sentinel-1 L1C GRD products and readily available on cloud computing platforms, such as Google Earth Engine or Amazon Web Services. When looking at the results achieved here, it becomes evident, however, that using intensity only limits the quality of the classification outcome for land cover mapping significantly. Comparing the results from Table III in rows 1–6 and 15–23, coherence always performs better even when only using the minimum baselines. The latter are also presented in Fig. 7. Especially interesting is the fact that using both the multitemporal coherence matrix and the multitemporal intensity simultaneously increases the result quality by up to 7%. This behavior was visible in basically all submitted results including the pixel and object domain.

C. Single Versus Dual Polarization Classification

Among all the results submitted to the RR evaluation, where the different polarimetric channels were tested separately, it became evident that they behave differently. The channel VV is the one that offers the best classification result. This was expected since the copolar channel VV exhibits a higher SNR than channel VH, as also demonstrated in the class samples of Fig. 1, where the behavior of six different land cover types is highlighted in both polarimetric channels. However, when both channels are processed jointly, the accuracy of the classification

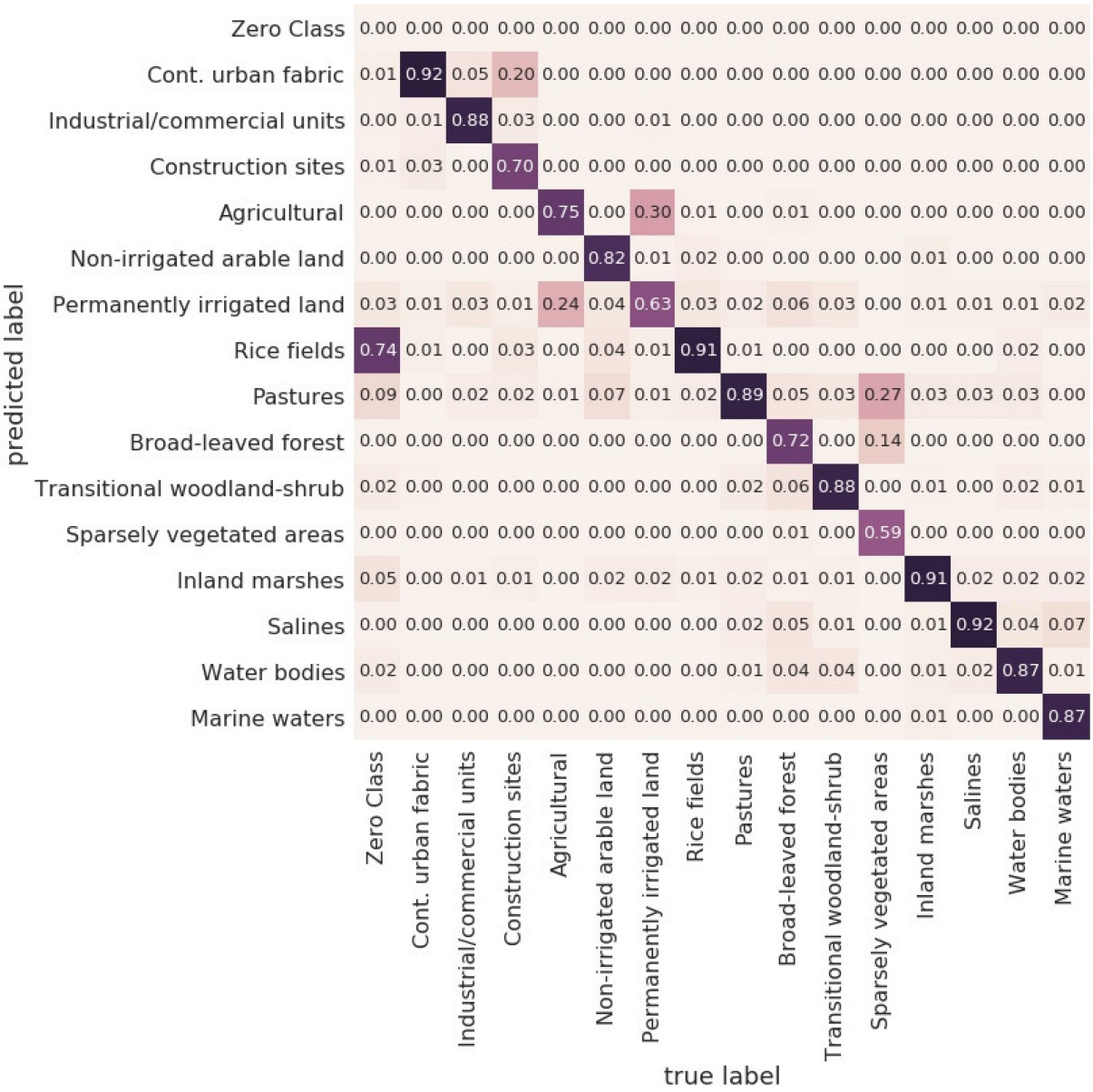

Fig. 5. Confusion matrix of best KTH-SEG result for Doñana, Spain. All values are given as a ratio between the number of pixels of predicted class and reference class.

increases, as can be seen in Table III rows 1–3 and 15–17. This is observed for both the coherence-based classification results as well as the intensity-based classification results, or the combination of both. In all cases, including both polarizations into the feature space of the classifiers yielded the best results, with improvements of 1%–5% in OA with respect to individual usage of one polarization.

D. Selecting the Number of Training Samples

Regarding the sampling strategy, the most prominent impact is the dependency on the number of training samples used for the machine-learning algorithms applied later. A comparison was made using the object-based approach of KTH-SEG with the support vector machine as the classifier and the outcome of this is visible in rows 27–29 in Table III. For all the study areas, it is clearly visible that, the more samples are used, the better the final results are in terms of OA.

E. Effects of Segmentation in the Classification Results

Among the different approaches of image classification, two were based on segmentation prior to classification. Both approaches significantly improved the OA. Fig. 8 shows a direct comparison using the KTH-SEG [7] approach and the standard RF approach in a pixel-based manner for all the three study areas. The improvements when applying the same input datasets and training samples are 4%–7%. (See also Table III, rows 25 and 26).

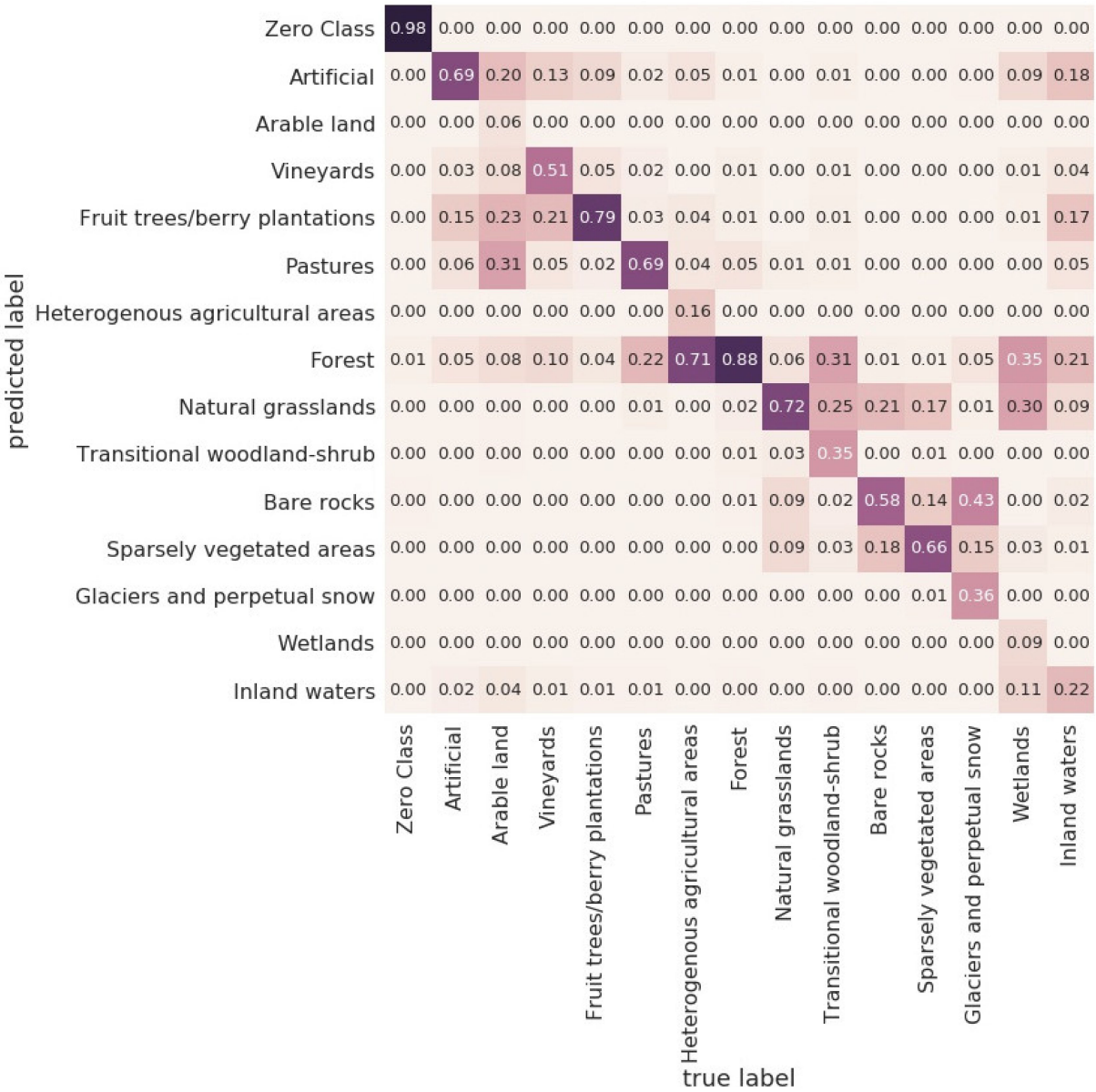

Fig. 6. Confusion matrix of best KTH-SEG result for Merano, South Tyrol, Italy. All values are given as a ratio between the number of pixels of predicted class and reference class.

F. Summary

The analysis performed in this article proved that key features and parameters exist that have a direct impact on the classification performance. The following list provides a summary of the insights detected and presented in this section.

1) Temporal Baseline: Results show that there is very limited improvement when more than the shortest baselines are considered. However, the seasonal effects, visible in the multitemporal coherence matrix in Fig. 1, suggest that there is some land cover information in larger baselines. Further analysis, including six-day baselines from S-1 A/B configuration, must provide more light in this regard.

2) Image Intensity and Interferometric Coherence: In this article, it has been shown that the coherence provides better results than the image intensities systematically in all evaluated cases. This is a remarkable fact that proves and might justify, depending on the application and the final requirements, the computation expense of the interferometric generation. It has also been detected that both features are complementary, improving results' accuracy in all cases when both are combined.

3) Polarization: A different sensitivity of both polarimetric channels has been observed. The VV component always provides better results than the VH counter part. The combination of both channels proves to be complementary. The S-1 polarimetric capabilities prevent an in-depth analysis in this direction.

4) Sampling: It has been shown how the number of samples influences the classification performances. This is a well known

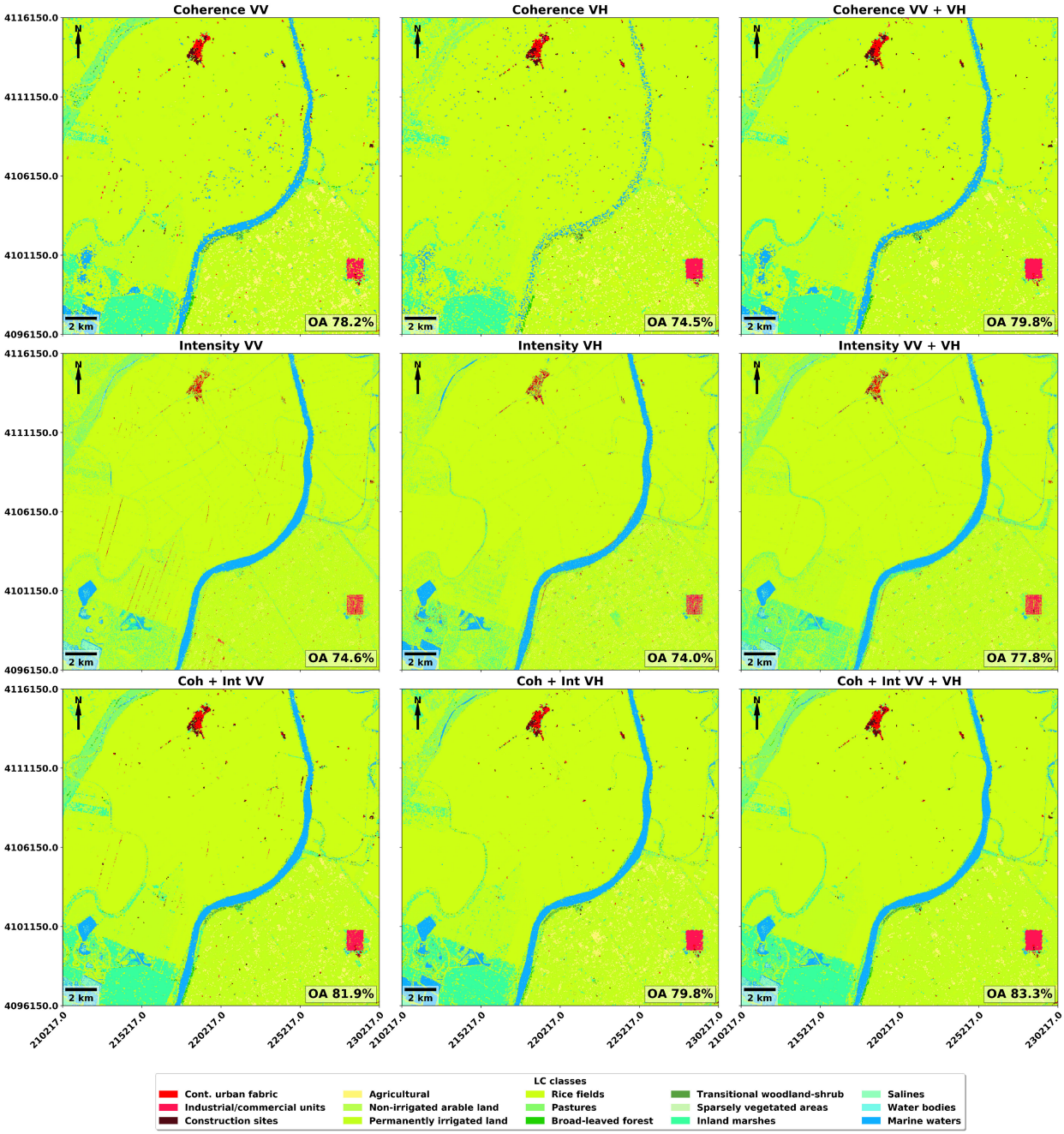

Fig. 7. Comparison of different Sentinel-1 SAR-based input features for classification in the Doñana site with 16 classes using the eigenvalue classification strategy. In the horizontal direction, the effects of the polarization can be observed while in the vertical direction the effects of considering the coherence, intensity, or both simultaneously are represented [for reference, see Fig. 4(a) and (d)].

characteristic in the classification domain, which also controls the capabilities of the methodology to generalize. Reasonably high accuracies are obtained with 1% of the total number of samples considering one or two campaigns. However, the generalization capabilities along the temporal dimension, i.e., extending the classification along the 2017 and 2018 campaigns, must still be analyzed in detail.

5) Segmentation: In general, object-based results show higher OA than the equivalent pixel-based maps. Although the maps produced using segmented coherences produce results (both qualitatively and quantitatively) closer to the ground truth, it can be seen that a finer detail is preserved in all pixel-based maps. This again stresses the importance of the definition and nature of the ground truth reference data used within the classification methodology.

V. Conclusion

In this article, the value of Sentinel-1 interferometric coherence for land cover mapping was analyzed and demonstrated.

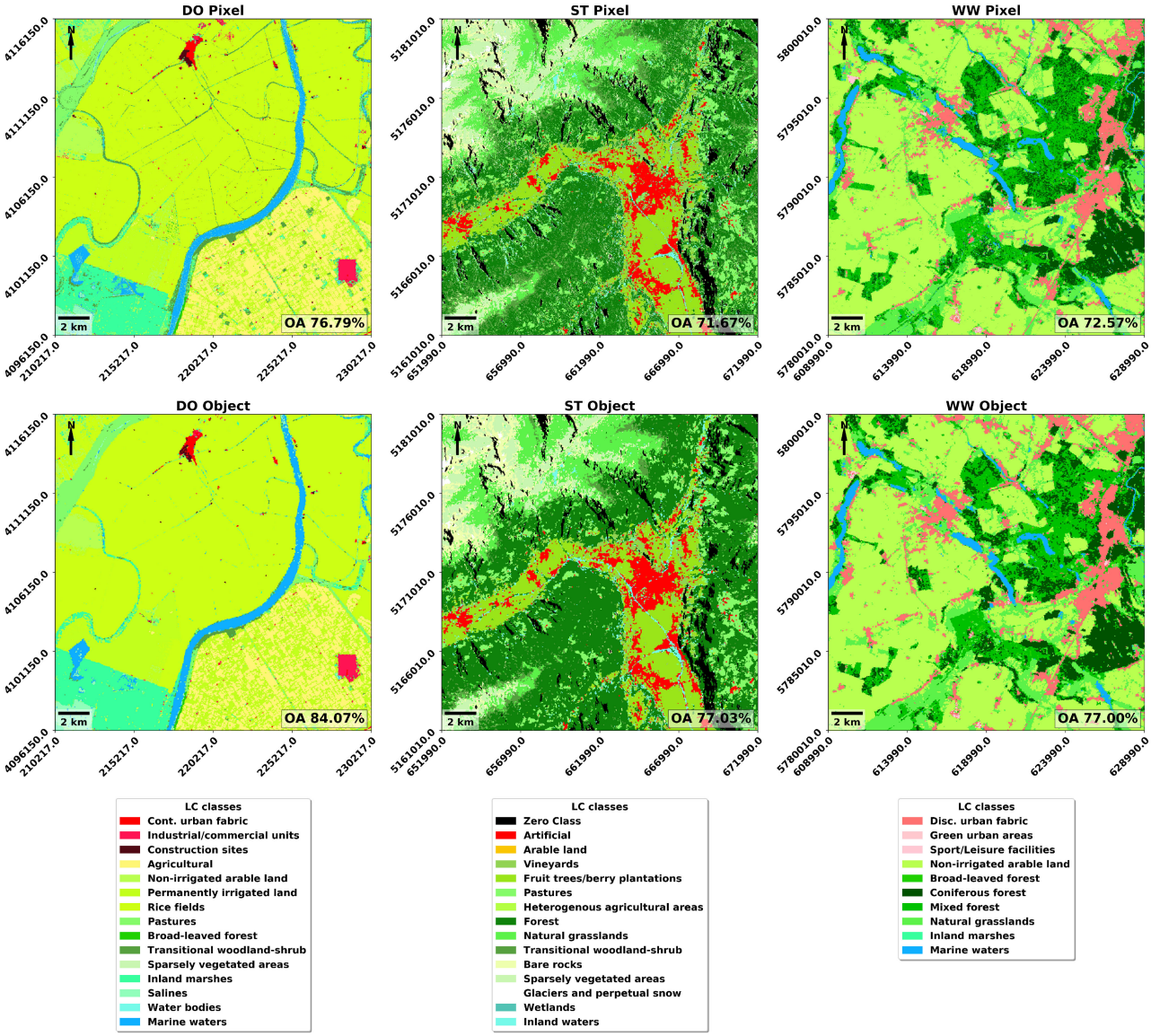

Fig. 8. Comparison of pixel-based and object-based classification results based on the object-based image classification (KTH-SEG). Row 1: Pixel-based results from left: Doñana (15 classes), middle: Merano (15 classes), right: West-Wielkopolska (9 classes). Row 2: Object-based results from left: Doñana (15 classes), middle: Merano (15 classes), right: West-Wielkopolska (9 classes). The zero class indicates layover and foreshortening effects due to the side-looking geometry in a strong topography.

A plethora of different classification strategies were applied, maintaining comparability by giving all participating research groups access to exactly the same set of analysis-ready input data. First and foremost, the results of this study indicate that the interferometric coherence provided in multitemporal matrices is a formidable source of information for land cover mapping, as has been proven by the fact that three different methodologies, developed by three different research groups, produced an OA of over 75% for all three study areas. It should be highlighted that in all study areas, nine or more classes were present, covering almost every class from the CORINE classification scheme. Further, the authors looked into the impact of different features and processing steps. Coherence is shown to perform better than intensity in all the evaluated scenarios, although this analysis shows that it is important and beneficial to include both intensity and coherence as both observables are complementary. A similar consequence is also deducted for the polarimetric channels, although VV systematically provides better accuracies. Further, it is enough to work with only a limited number of multitemporal baselines and for all machine-learning approaches, the number of training samples provided has the biggest impact. Finally, object-based approaches performed significantly better than pixel-based approaches in terms of thematic accuracy, but tended to lose some geometric detail. Future analysis will now focus on performing classifications over larger areas in order to study the general applicability of the interferometric coherence for land cover mapping further. Also, the impact of the now readily available six-day coherence for the years 2017 and 2018 will certainly further improve the capability of this SAR-derived feature for classification purposes, especially in the vegetation

domain, where higher temporal variability can be expected. In addition, the comparison between SAR- and optical-based land cover products and a data assimilation framework to exploit both domains simultaneously will be evaluated in future studies. Finally, this study has confirmed the capabilities of the interferometric coherence for land cover classification. The common concerns with using interferometric products from an operational standpoint are usually related to the computational requirements when compared to SLC images or optical products. In the RR experience, the provision of analysis-ready data easily resolved the main drawback providing a relevant feature into the classification scheme. Although a deeper evaluation on the computational cost must be addressed, from the classification perspective, the necessity of a ready-to-use coherence feature has been clearly revealed.

ACKNOWLEDGMENT

The authors would like to thank B. Ventura for organizing the efficient access to the Sentinel-1 SLC data and L. Cattani for his efforts of setting up the Jupyter-hub environment.

REFERENCES

[1] A. Huff, "GEO task US-09-01a: Critical earth observations priorities," Group Earth Observ., Geneva, Switzerland, Tech. Rep., 2012. [Online]. Available: https://sbageotask.larc.nasa.gov/Disasters_Pt2_US0901a-FINAL.pdf

[2] M. C. Dobson, F. T. Ulaby, and L. E. Pierce, "Land-cover classification and estimation of terrain attributes using synthetic aperture radar," *Remote Sens. Environ.*, vol. 51, no. 1, pp. 199–214, 1995.

[3] M. C. Dobson, L. E. Pierce, and F. T. Ulaby, "Knowledge-based land-cover classification using ERS-1/JERS-1 SAR composites," *IEEE Trans. Geosci. Remote Sens.*, vol. 34, no. 1, pp. 83–99, Jan. 1996.

[4] H. Hu and Y. Ban, "Urban land-cover mapping and change detection with Radarsat SAR data using neural network and rule-based classifiers," *Int. Arch. Photogramm. Rem. Sens. Spatial Info. Sci*, vol. 37, pp. 1549–1554, 2008.

[5] B. Waske and M. Braun, "Classifier ensembles for land cover mapping using multitemporal SAR imagery," *ISPRS J. Photogramm. Remote Sens.*, vol. 64, no. 5, pp. 450–457, 2009.

[6] P. Mishra, D. Singh, and Y. Yamaguchi, "Land cover classification of PALSAR images by knowledge based decision tree classifier and supervised classifiers based on SAR observables," *Prog. Electromagn. Res.*, vol. 30, pp. 47–70, 2011.

[7] Y. Ban and A. Jacob, "Object-based fusion of multitemporal multiangle ENVISAT ASAR and HJ-1B multispectral data for urban land-cover mapping," *IEEE Trans. Geosci. Remote Sens.*, vol. 51, no. 4, pp. 1998–2006, Apr. 2013.

[8] T. Strozzi *et al.*, "Landuse mapping with ERS SAR interferometry," *IEEE Trans. Geosci. Remote Sens.*, vol. 38, no. 2, pp. 766–775, Mar. 2000.

[9] M. E. Engdahl and J. M. Hyyppa, "Land-cover classification using multitemporal ERS-1/2 InSAR data," *IEEE Trans. Geosci. Remote Sens.*, vol. 41, no. 7, pp. 1620–1628, Jul. 2003.

[10] L. Matikainen, J. Hyyppä, and M. E. Engdahl, "Mapping built-up areas from multitemporal interferometric SAR images-a segment-based approach," *Photogramm. Eng. Remote Sens.*, vol. 72, no. 6, pp. 701–714, 2006.

[11] M. Santoro, J. I. Askne, U. Wegmuller, and C. L. Werner, "Observations, modeling, and applications of ERS-ENVISAT coherence over land surfaces," *IEEE Trans. Geosci. Remote Sens.*, vol. 45, no. 8, pp. 2600–2611, Aug. 2007.

[12] R. Abdelfattah and J.-M. Nicolas, "Mixture model for the segmentation of the InSAR coherence map," *Int. J. Appl. Earth Observ. Geoinf.*, vol. 12, pp. S138–S144, 2010.

[13] N. Joshi *et al.*, "Mapping dynamics of deforestation and forest degradation in tropical forests using radar satellite data," *Environ. Res. Lett.*, vol. 10, no. 3, 2015, Art. no. 034014.

[14] N. Joshi *et al.*, "A review of the application of optical and radar remote sensing data fusion to land use mapping and monitoring," *Remote Sens.*, vol. 8, no. 1, 2016, Art. no. 70.

[15] T. Tamm, K. Zalite, K. Voormansik, and L. Talgre, "Relating Sentinel-1 interferometric coherence to mowing events on grasslands," *Remote Sens.*, vol. 8, no. 10, 2016, Art. no. 802.

[16] M. Chini, R. Pelich, R. Hostache, P. Matgen, and C. Lopez-Martinez, "Towards a 20 m global building map from Sentinel-1 SAR data," *Remote Sens.*, vol. 10, no. 11, 2018, Art. no. 1833.

[17] S. R. Cloude and E. Pottier, "An entropy based classification scheme for land applications of polarimetric SAR," *IEEE Trans. Geosci. Remote Sens.*, vol. 35, no. 1, pp. 68–78, Jan. 1997.

[18] J.-S. Lee, M. R. Grunes, and E. Pottier, "Quantitative comparison of classification capability: Fully polarimetric versus dual and single-polarization SAR," *IEEE Trans. Geosci. Remote Sens.*, vol. 39, no. 11, pp. 2343–2351, Nov. 2001.

[19] X. Niu and Y. Ban, "Multi-temporal RADARSAT-2 polarimetric SAR data for urban land-cover classification using an object-based support vector machine and a rule-based approach," *Int. J. Remote Sens.*, vol. 34, no. 1, pp. 1–26, 2013.

[20] R. Bamler and P. Hartl, "Synthetic aperture radar interferometry," *Inverse Problems*, vol. 14, no. 4, p. R1, 1998.

[21] E. Rodriguez and J. M. Martin, "Theory and design of interferometric synthetic aperture radars," *IEE Proc. F - Radar Signal Process.*, vol. 139, no. 2, pp. 147–159, Apr. 1992.

[22] H. A. Zebker and J. Villasenor, "Decorrelation in interferometric radar echoes," *IEEE Trans. Geosci. Remote Sens.*, vol. 30, no. 5, pp. 950–959, Sep. 1992.

[23] M. S. Seymour and I. G. Cumming, "Maximum likelihood estimation for SAR interferometry," in *Proc. IEEE Int. Geosci. Remote Sens. Symp.*, Aug. 1994, vol. 4, pp. 2272–2275.

[24] M. Ragan-Kelley *et al.*, "The Jupyter/IPython architecture: A unified view of computational research, from interactive exploration to communication and publication," in *Proc. AGU Fall Meet.*, 2014. [Online]. Available: https://abstractsearch.agu.org/meetings/2014/FM/H44D-07.html

[25] T. Kluyver *et al.*, "Jupyter notebooks—A publishing format for reproducible computational workflows," in *Proc. Int. Conf. Electron. Publishing*, 2016, pp. 87–90.

[26] R. Bürgmann, P. A. Rosen, and E. J. Fielding, "Synthetic aperture radar interferometry to measure earth's surface topography and its deformation," *Annu. Rev. Earth Planet. Sci.*, vol. 28, no. 1, pp. 169–209, 2000.

[27] N. Yague-Martinez, F. D. Zan, and P. Prats-Iraola, "Coregistration of interferometric stacks of Sentinel-1 TOPS data," *IEEE Geosci. Remote Sens. Lett.*, vol. 14, no. 7, pp. 1002–1006, Jul. 2017.

[28] D. Carrasco, "SAR Interferometry for digital elevation model generation and differential applications," Ph.D. dissertation, Universitat Politécnica de Catalunya, Mar. 1998.

[29] A. Jacob *et al.*, "Organizing access to complex multi-dimensional data: An example from the ESA SEOM SInCohMap project," in *Proc. Conf. Big Data From Space*, 2017, pp. 205–208.

[30] P. Baumann, A. Dehmel, P. Furtado, R. Ritsch, and N. Widmann, "The multidimensional database system RasDaMan," *ACM Sigmod Rec.*, vol. 27, no. 2, pp. 575–577, 1998.

[31] P. Baumann, A. M. Dumitru, and V. Merticariu, "The array database that is not a database: File based array query answering in rasdaman," in *Proc. Int. Symp. Spatial Temporal Databases*, 2013, pp. 478–483.

[32] M. J. Canty, *Image Analysis, Classification and Change Detection in Remote Sensing: With Algorithms for ENVI/IDL and Python*. Boca Raton, FL, USA: CRC Press, 2014.

[33] F. Pedregosa *et al.*, "Scikit-learn: Machine learning in Python," *J. Mach. Learn. Res.*, vol. 12, pp. 2825–2830, Oct. 2011.

[34] C. Homer, C. Huang, L. Yang, B. Wylie, and M. Coan, "Development of a 2001 national land-cover database for the United States," *Photogramm. Eng. Remote Sens.*, vol. 70, no. 7, pp. 829–840, 2004.

[35] J. O. Sexton, D. L. Urban, M. J. Donohue, and C. Song, "Long-term land cover dynamics by multi-temporal classification across the Landsat-5 record," *Remote Sens. Environ.*, vol. 128, pp. 246–258, 2013.

[36] P. Virtanen *et al.*, "SciPy 1.0-Fundamental Algorithms for Scientific Computing in Python," 2019, *preprint arXiv:1907.10121*.

[37] T. E. Oliphant, *A Guide to NumPy*, vol. 1. USA: Trelgol Publishing, 2006.

[38] N. R. Lomb, "Least-squares frequency analysis of unequally spaced data," *Astrophys. Space Sci.*, vol. 39, no. 2, pp. 447–462, 1976.

[39] J. D. Scargle, "Studies in astronomical time series analysis. II—Statistical aspects of spectral analysis of unevenly spaced data," *Astrophys. J.*, vol. 263, pp. 835–853, 1982.

[40] L. Breiman, "Random forests," *Mach. Learn.*, vol. 45, no. 1, pp. 5–32, 2001.
[41] K. Millard and M. Richardson, "On the importance of training data sample selection in random forest image classification: A case study in peatland ecosystem mapping," *Remote Sens.*, vol. 7, no. 7, pp. 8489–8515, 2015.
[42] A. Jacob, "Multitemporal remote sensing for urban mapping using KTH-SEG and KTH-Pavia urban extractor," Ph.D. dissertation, , KTH Roy. Inst. Technol., Stockholm, Sweden, 2014.
[43] R. C. Gonzalez and R. E. Woods, *Digital Image Processing*, 2nd ed. Boston, MA, USA: Addison-Wesley Longman, 2001.
[44] R. Achanta, A. Shaji, K. Smith, A. Lucchi, P. Fua, and S. Süsstrunk, "SLIC superpixels compared to state-of-the-art superpixel methods," *IEEE Trans. Pattern Anal. Mach. Intell.*, vol. 34, no. 11, pp. 2274–2282, Nov. 2012.
[45] O. Antropov, Y. Rauste, T. Häme, and J. Praks, "Polarimetric ALOS PALSAR time series in mapping biomass of boreal forests," *Remote Sens.*, vol. 9, no. 10, 2017, Art. no. 999.
[46] M. A. Friedl and C. E. Brodley, "Decision tree classification of land cover from remotely sensed data," *Remote Sens. Environ.*, vol. 61, no. 3, pp. 399–409, 1997.
[47] S. V. Stehman, "Selecting and interpreting measures of thematic classification accuracy," *Remote Sens. Environ.*, vol. 62, no. 1, pp. 77–89, 1997.
[48] C.-A. Deledalle, L. Denis, and F. Tupin, "NL-InSAR: Nonlocal interferogram estimation," *IEEE Trans. Geosci. Remote Sens.*, vol. 49, no. 4, pp. 1441–1452, Apr. 2011.
[49] A. Ferretti, A. Fumagalli, F. Novali, C. Prati, F. Rocca, and A. Rucci, "A new algorithm for processing interferometric data-stacks: SqueeSAR," *IEEE Trans. Geosci. Remote Sens.*, vol. 49, no. 9, pp. 3460–3470, Sep. 2011.
[50] A. Parizzi and R. Brcic, "Adaptive InSAR stack multilooking exploiting amplitude statistics: A comparison between different techniques and practical results," *IEEE Geosci. Remote Sens. Lett.*, vol. 8, no. 3, pp. 441–445, May 2011.
[51] J. Kang, Y. Wang, and X. X. Zhu, "Multi-pass SAR interferometry for 3D reconstruction of complex mountainous areas based on robust low rank tensor decomposition," in *Proc. IEEE Int. Geosci. Remote Sens. Symp.*, 2018, pp. 8703–8706.

Alexander W. Jacob (Member, IEEE) received the licentiate degree in geoinformatics.

He coordinates the research group Advanced Computing for Earth Observation, within the Institute for Earth Observation with the objective to foster EO data science by actively contributing to research in regional and international projects, fully capitalizing on EO data in the space, time, and feature domains. He is an experienced Researcher and Software Developer in the field of earth observation (more than five years of experience). He is responsible for scientific data management including the organization of multidimensional raster data and coordination of algorithm development in operational and research processing chains. He is currently an active Project Manager for Eurac Research's contribution to the H2020 openEO Project and the ESA SEOM SInCohMap Project as well as several internal development projects.

Fernando Vicente-Guijalba (Member, IEEE) was born in Alicante, Spain, in 1981. He received the bachelor's and M.Sc. degrees in telecommunications engineering and the Ph.D. degree in computer science from the University of Alicante, Alicante, Spain, in 2011, 2014, and 2016, respectively.

From 2011 to 2016, he was a Junior Researcher with the Signals, Systems and Telecommunications (SST) Group, University of Alicante, acquiring solid experience in academic and operational research in the remote sensing analysis and processing field for earth observation monitoring. Since 2017, he has been with Dares Technology, Barcelona, Spain, and since 2019, he has been leading the institutional projects division of the company. His current research interests include the application of multispectral and radar data for land cover and vegetation mapping.

Carlos Lopez-Martinez (Senior Member, IEEE) received the M.Sc. degree in electrical engineering and the Ph.D. degree from the Universitat Politécnica de Catalunya, Barcelona, Spain, in 1999 and 2003, respectively.

He is currently an Associate Professor in the area of remote sensing and microwave technology with the Universitat Politécnica de Catalunya. He also has a wide professional international experience. From October 2000 to March 2002, he was with the High Frequency and Radar Systems Department, HR, German Aerospace Center, DLR, Oberpfaffenhofen, Germany. From June 2003 to December 2005, he has been with the Image and Remote Sensing Group SAPHIR Team, Institute of Electronics and Telecommunications of Rennes (I.E.T.R. CNRS UMR 6164), Rennes, France. Finally, from May 2017 until September 2019 he was responsible for the Remote Sensing and Natural Resources Modelling Group, Luxembourg Institute of Science and Technology, Esch-sur-Alzette, Luxembourg. He has organized different invited sessions in international conferences on radar and SAR polarimetry. He has presented advanced courses and seminars on radar polarimetry to a wide range of organizations and events. He is the author or co-author of more than 150 articles in journals, books, and conference proceedings in the radar remote sensing and image analysis literature. His research interests include SAR and multidimensional SAR, radar polarimetry, physical parameter inversion, digital signal processing, estimation theory, and harmonic analysis.

Dr. Lopez-Martinez was the recipient of the Student Prize Paper Award at the EUSAR 2002 Conference and was co-author of the paper awarded with the First Place Student Paper Award at the EUSAR 2012 Conference. He was also the recipient of the IEEE-GRSS 2013 GOLD Early Career Award. He is an Associate Editor for the IEEE JOURNAL OF SELECTED TOPICS IN APPLIED EARTH OBSERVATIONS AND REMOTE SENSING and *MDPI Remote Sensing*. He was a Guest Editor for the *EURASIP Journal on Advances in Signal Processing*.

Juan M. Lopez-Sanchez (Senior Member, IEEE) was born in Alicante, Spain, in 1972. He received the Ingeniero (M.S.) and Doctor Ingeniero (Ph.D.) degrees in telecommunication engineering from the Technical University of Valencia (UPV), Valencia, Spain, in 1996 and 2000, respectively.

From 1998 to 1999, he was a Predoctoral Grantholder with the Space Applications Institute, Joint Research Centre of the European Commission, Ispra, Italy. Since 2000, he has been leading the Signals, Systems and Telecommunication Group, University of Alicante, Alicante, Spain, where he has been a Full Professor since November 2011. He has coauthored more than 70 papers in refereed journals and more than 120 papers and presentations in international conferences and symposia. His main research interests include microwave remote sensing for inversion of biophysical parameters, polarimetric and interferometric techniques, SAR imaging algorithms, and applications of radar remote sensing in agriculture and geophysics.

Dr. Lopez-Sanchez was the recipient of the Indra Award for the Best Ph.D. Thesis About Radar in Spain, in 2001. From 2006 to 2012, he was the Chair of the Spanish Chapter of the IEEE Geoscience and Remote Sensing Society.

Marius Litzinger was born in 1991. He received the M.Sc. degree in physical geography from the Philipps-Universitt Marburg, Marburg, Germany, in 2019.

From February to August 2018, he was Trainee with the Eurac Research Institute for Earth Observation, Bolzano, Italy. He is now a GIS-Analyst with the Environmental Planning Agency TNL Energie GmbH, Hungen, Germany.

Harald Kristen received the B.Sc. degree in environmental system sciences, focusing on geoinformatics from the University of Graz, Graz, Austria, in 2015, and the master's degree from the Institute for Earth Observation, Eurac Research, Bolzano, Italy, working on the application of the data cube concept for multi temporal satellite imagery.

He is currently with Festmeter.at, Leoben, Austria, a digital startup in the forestry sector. His current project is early detection of bark beetle infestation in spruce forests. He research interests include remote sensing with UAV and aerial imagery, geoinformatics, and artificial intelligence.

Alejandro Mestre Quereda (Member, IEEE) was born in Madrid, Spain, in 1990. He received the B.S. and M.Sc. degrees in telecommunication engineering and the Ph.D. degree from the University of Alicante (UA), Alicante, Spain, in 2015, 2017, and 2019, respectively.

He is currently a Postdoctoral Researcher with the Signals, Systems and Telecommunication (SST) Group, UA. His research interests include the development of advanced signal processing techniques for SAR interferometry and polarimetry, and the exploitation of SAR/InSAR data for new applications including land-cover and vegetation mapping.

Dariusz Ziółkowski received the Ph.D. degree in earth science.

He is the Head of the Microwave Remote Sensing Laboratory, Remote Sensing Centre, Institute of Geodesy and Cartography, Warsaw, Poland. He has 18 years of experience in EO science. He has also experience in managing of EO research projects. His main research interests include the integration of various geodetic techniques for deformation studies and the study of synergy of polarimetry and backscattering coefficient for better estimation of biophysical parameters of forests from SAR data.

Marco Lavalle received the M.Sc. degree in telecommunication engineering from the University of Rome Tor Vergata, Rome, Italy, in 2006, and the Ph.D. degree from the University of Rennes 1, Rennes, France, and from the University of Rome Tor Vergata, Rome, Italy, in December 2009.

He is a Scientist with the NASA Jet Propulsion Laboratory, California Institute of Technology, Pasadena, CA, USA. From 2006 to 2008, he was a Visiting Scientist with the European Space Agency (ESRIN), Paris, France, where he supported ESA's activities on polarimetric radar calibration and polarimetric radar interferometry science-algorithm development. From January 2010 to December 2011, he was NASA Postdoctoral Fellow with the Jet Propulsion Laboratory (JPL), California Institute of Technology. Since January 2012, he has been a Permanent Scientist with the JPL Radar Science and Engineering Section. He has been Principal Investigator and Coinvestigator for several NASA programs. He is a Member of the NISAR, UAVSAR, CYGNSS, and ROSE-L Science Teams. His research interests include retrieval algorithm development, physical and statistical model formulation, electromagnetic propagation, scattering theory, SAR tomography, polarimetric SAR interferometry, land parameter characterization, ecosystem modeling, and parameter estimation.

Dr. Lavalle is the recipient of the 2019 NASA Early Career Public Achievement Medal, the 2020 JPL Lew Allen Award for Excellence, and the Student Prize Paper Award at the EUSAR 2008 Conference (Friedrichshafen, Germany).

Claudia Notarnicola (Member, IEEE) received the M.S. degree in physics (summa cum laude) and the Ph.D. degree in physics from the University of Bari, Bari, Italy, in 1995 and 2002, respectively.

She is currently the Vice Head of the Institute for Earth Observation, EURAC Research Center, Bolzano, Italy. Within the same institute, she is also the leader of a group dealing with remote sensing applications in the synthetic aperture radar (SAR) and optical domain for soil, snow, and vegetation monitoring as well as integration of remotely sensed observations with models and ground measurements. She conducts research on her topics of interest within the frameworks of several national and international projects. Among others, she was also involved in the CassiniHuygens Mission for the application of an inversion procedure to the estimation of Titan surface parameters. Her main research interests include biophysical parameter (soil moisture, vegetation, and snow) retrieval using optical and SAR images, optical and SAR data processing, data fusion, and electromagnetic models.

Dr. Notarnicola has been a Conference Chair for the SPIE International Conference on Active and Passive Microwave Remote Sensing for Environmental Monitoring since 2006.

Gopika Suresh was born in Kerala, India, in 1987. She received the B.Tech. degree in electronics and communications engineering from the University of Kerala, Thiruvananthapuram, India, in 2009, the M.Sc. degree in earth oriented space science and technology (ESPACE) from the Technical University of Munich, Munich, Germany, and the Ph.D. degree (Dr. rer. Nat) in geosciences from the University of Bremen, Bremen, Germany, in 2015, where she implemented the first automatic algorithm for the estimation of natural offshore oil seeps and detection of natural oil slicks from synthetic aperture radar (SAR) data.

From 2015 to 2019, she was with the German Federal Agency for Cartography and Geodesy (BKG), Frankfurt, Germany, and was responsible for the project "Land Cover Classification from Sentinel-1 Data" within which she used techniques such as texture extraction, multitemporal analysis, PolSAR, and InSAR. From 2018 to 2019, she was responsible for the project "Cop4SDGs" where she worked together with the German Environmental Agency to implement methods to estimate the sustainable development goal (SDG) indicators using Copernicus data. She is currently an MTG Systems Engineer with EUMETSAT, through the company CS Communication and Systems Germany GmbH, Darmstadt, Germany. Her research interests include application of SAR and EO data for disaster management, land cover mapping, natural oil slick detection, and SDGs.

Oleg Antropov (Member, IEEE) was born in Almaty, Kazakhstan, in 1984. He received the M.S. degree in computer science and the Candidate of Sciences degree in radio physics from Dnipropetrovsk National University, Dnipropetrovsk, Ukraine, in 2006 and 2010, respectively, and the Ph.D. degree in space technology from Aalto University, Espoo, Finland, in 2014.

Since 2010, he has been with the Remote Sensing Group, VTT Technical Research Centre of Finland, Espoo, Finland, as a Research Scientist and Senior Scientist. He was also a Postdoctoral Associate with Aalto University during 2014–2018, and a Research Consultant with ICEYE in 2018. His research interests include the application of multiparameteric SAR data for various environmental applications, most centrally forestry and crops.

Shaojia Ge was born in Zhenjiang, China, in June 1991. He received the B.Eng. degree in electronic information engineering, in 2013, from the Nanjing University of Science and Technology, Nanjing, China, where he is currently working toward the Ph.D. degree in radar signal processing with the School of Electronic and Optical Engineering.

In 2008, he was a Visiting Student with the Department of Electronics and Nanoengineering, Aalto University, Espoo, Finland. His research interests include SAR remote sensing, especially on PolSAR image segmentation and land cover classification.

Jaan Praks, received the M.Sc. degree in physics from the University of Tartu, Tartu, Estonia and the Ph.D. degree in space technology from Aalto University, Espoo, Finland, 2012.

He is an Assistant Professor (tenure track) with Aalto University and a Leader of Aalto Space Technology and Microwave Remote Sensing research group. During his career, he has participated in numerous remote sensing projects and measurement campaigns, instrument developments and led the development of Aalto-1, Aalto-2, Aalto-3, and Foresail nanosatellites. He is currently leading Satellite Platforms team in Finnish Centre of Excellence in Research of Sustainable Space. From his research projects have started many New Space and Earth Observation start-up companies in Finland. His research interests include microwave remote sensing, especially SAR Interferometry and SAR polarimetry, and nanosatellite technology.

Yifang Ban (Member, IEEE) received the B.Sc. and M.Sc. degrees from Nanjing University, China, and the Ph.D. degree from the University of Waterloo, Waterloo, ON, Canada, in 1996.

She is a Professor and the Director of the Geoinformatics Division, KTH Royal Institute of Technology, Stockholm, Sweden. Before joining KTH in 2004, he was a Tenured Associate Professor with York University, Toronto, ON, Canada. She is a Co-Lead of the Group on Earth Observations (GEO) initiative "Global Urban Observation and Information," and a Co-Chair for ICA Commission on Sensor-Driven Mapping. She is the Lead PI for the ESA INNOVATOR III Project "EO4Urban" and the European Lead PI for the Project "EO4SmartCities" within the ESA/China Dragon 4 Program, among others. She is also an Invited Expert for the UN Habitat's Technical Committee on Human Settlements Indicators for UN Sustainable Development Goals (SDGs). Her research interests include multitemporal SAR and optical image processing, earth observation (EO) big data analytics, and their applications in urban and land cover mapping, urbanization, wildfire, and other environmental change monitoring, environmental impact assessment, disaster damage assessment and decision support, among others, and has published extensively on these topics.

Dr. Ban has been an Associate Editor and Guest Editor for major remote sensing journals and an Invited Expert for EU and national grant application evaluations.

Eric Pottier (Fellow, IEEE) received the M.Sc. and Ph.D. degrees in signal processing and telecommunication from the University of Rennes 1, Rennes, France, in 1987 and 1990, respectively, and the habilitation from the University of Nantes, Nantes, France, in 1998.

Since 1999, he has been a Full Professor with the University of Rennes 1 in analog electronics, signal processing, and telecommunications. He has supervised more than 60 research students to graduation (M.Sc. and Ph.D.) in radar polarimetry and remote sensing applications. He has coauthored a book *Polarimetric Radar Imaging: From Basics to Applications* (CRC Press, Taylor & Francis, 2009) with Dr. J. S. Lee. His research interests cover a wide spectrum of areas from radar image processing (SAR, ISAR) to fundamentals and basic theory of radar polarimetry.

Dr. Pottier was the recipient of the Award for a Very Significant Contribution in the Field of Synthetic Aperture Radar during EUSAR2000, the 2007 IEEE GRS-S Letters Prize Paper Award, the 2007 IEEE GRS-S Education Award in recognition of his significant educational contributions to geoscience and remote sensing, the 2012 Einstein Professorship from the Chinese Academy of Science, and the CNFRS-URSI Medal under the auspices of the French Academy of Sciences in 2015. He was recognized as an IEEE GRS-S Distinguished Lecturer in 2014. He has been elevated to IEEE Fellow (January 2011) with the accompanying citation: "for contributions to polarimetric synthetic aperture radar."

Jordi Joan Mallorqui Franquet (Senior Member, IEEE) was born in Tarragona, Spain, in 1966. He received the Ingeniero and Doctor Ingeniero degrees in telecommunications engineering from the Universitat Politcnica de Catalunya (UPC), Barcelona, Spain, in 1990 and 1995, respectively.

Since 1993, he has been an Assistant Professor with the School of Telecommunications Engineering of Barcelona, UPC, where he became an Associate Professor in 1997, and has been a Full Professor since 2011. Since November 2018, he has been the Head of the Signal Theory and Communications Department, UPC. His teaching activity involves microwaves, radio navigation systems, and remote sensing. He spent a sabbatical year with the Jet Propulsion Laboratory, Pasadena, CA, USA, in 1999, where he was involved with interferometric airborne synthetic aperture radar (SAR) calibration algorithms. He has authored or coauthored more than 100 papers on microwave tomography, EM numerical simulation, and SAR processing, interferometry, and differential interferometry in refereed journals and international symposia. His current research interests include the application of SAR interferometry to terrain-deformation monitoring with orbital, airborne, and ground-based sensors, vessel detection and classification from SAR images, and 3-D electromagnetic (EM) simulation of SAR systems.

Javier Duro Calvo was born in Barcelona, Spain, in 1978. He received the bachelor's and M.Sc. degrees in telecommunications engineering from the Polytechnic University of Catalonia, Barcelona, Spain, and the Ph.D. degree in applied geomatics and remote sensing from the University of Marne-la-Valle, Paris, France, in 2001 and 2010, respectively.

From 2001 to 2015, he was with ALTAMIRA-INFORMATION as Radar Expert, acquiring a solid experience in remote sensing applications and international market developments. He also led research projects for new satellite mission and for earth observation monitoring for European Commission, CNES, and ESA. In 2015, he founded Dares Technology, Barcelona, Spain, where he is the CEO of the company. His research interests include the implementation of innovative business plan for commercializing earth observation services and products.

Marcus E. Engdahl (Member, IEEE) received the M.Sc. degree in technology (technical physics) from the Helsinki University of Technology, Helsinki, Finland, in 1996, and the D.Sc degree in technology (electrical engineering) from Aalto University, Helsinki, Finland, in 2013.

Since August 2003, he has been an Earth Observation Applications Engineer with ESA-ESRIN, Frascati, Italy. In 1999, he completed the Summer Session Course (Nakhon Ratchasima, Thailand) organized by the International Space University, Strasbourg, France. In ESA, he has been involved with algorithm development and scientific data utilization of ERS-1/2, Envisat, Sentinel-1, and CryoSat-2 missions. He is actively involved with the evolution of the Sentinel-1 mission and preparation for the BIOMASS mission. He is responsible for the ESA SNAP toolbox development, including Sentinel-1 Toolbox and its predecessor ESA NEST toolbox. His research interests include biogeophysical parameter retrieval from multitemporal InSAR data, scientific utilization of SAR and InSAR data, algorithm and software development, remote sensing of the cryosphere, glaciology, and monitoring of the polar ice sheets from space.